

# Synthesis and Preclinical Evaluation of a Folic Acid Derivative Labeled with $^{18}\text{F}$ for PET Imaging of Folate Receptor–Positive Tumors

Andrea Bettio<sup>1</sup>, Michael Honer<sup>1</sup>, Cristina Müller<sup>1</sup>, Matthias Brühlmeier<sup>2</sup>, Ursina Müller<sup>1</sup>, Roger Schibli<sup>1</sup>, Viola Groehn<sup>3</sup>, August P. Schubiger<sup>1</sup>, and Simon M. Ametamey<sup>1</sup>

<sup>1</sup>Department of Chemistry and Applied Biosciences of ETH, Center for Radiopharmaceutical Science of ETH, PSI, and USZ, Zurich, Switzerland; <sup>2</sup>Department of Nuclear Medicine, Cantonal Hospital, Aarau, Switzerland; and <sup>3</sup>Merck Eprova AG, Schaffhausen, Switzerland

Folic acid was linked regioselectively through its  $\alpha$ - and  $\gamma$ -carboxyl groups to 4-fluorobenzylamine (FBA), and the  $\alpha$ - and  $\gamma$ -FBA-folate regioisomers were evaluated for their ability to bind to folate receptor–positive cells. The  $^{18}\text{F}$ -labeled  $\alpha/\gamma$ -FBA-folate counterpart was examined for in vivo tumor targeting efficiency in nude mice bearing folate receptor–positive tumor cells. **Methods:**  $^{18}\text{F}$ - $\alpha/\gamma$ -FBA-folate was prepared in a 4-step reaction sequence starting from folic acid. The relative binding affinities of the  $\alpha$ - and  $\gamma$ -FBA-folates to the folate receptor with respect to parent folic acid were determined in cultured KB-31 cells (nasopharyngeal epidermal carcinoma cell line) overexpressing the folate receptor using  $^3\text{H}$ -folic acid. Tumor accumulation of the  $^{18}\text{F}$ -labeled  $\alpha/\gamma$ -FBA-folate and  $^{18}\text{F}$ -FDG was analyzed in vivo by high-resolution PET. Biodistribution and PET studies were performed under baseline and blockage conditions. **Results:** The radiochemical yield of the coupling step ranged from 15% to 44%, and the maximum specific radioactivity was 24 GBq/ $\mu\text{mol}$ . The in vitro binding affinities of the  $\alpha$ - and  $\gamma$ -isomers and folic acid were 71, 62, and 41 nmol/L, respectively. PET revealed heterogeneous uptake of the radioligand, with the highest activity concentrations found in the tumor rim. In contrast,  $^{18}\text{F}$ -FDG uptake in a nude mouse bearing KB-31 folate receptor–positive tumors was negligible. Radioligand uptake in tumors at 125 min after injection amounted to 6.56% of the injected dose per gram of tissue (%ID/g) in control animals, whereas radioactivity accumulation in the tumors of folic acid–treated animals was significantly reduced by more than 80%—to 1.07 %ID/g ( $P = 0.001$ ). **Conclusion:** This new  $^{18}\text{F}$ -labeled folic acid derivative is a promising tool for PET imaging of folate receptor–positive tumors.

**Key Words:** folate receptor;  $^{18}\text{F}$  labeling; PET; tumor imaging

**J Nucl Med 2006; 47:1153–1160**

**F**olic acid, also known as vitamin B9, is an essential dietary vitamin required by eukaryotic cells for 1-carbon

metabolism, DNA synthesis, and spinal canal and brain development during early pregnancy (1). Since the early 1990s, folic acid has become a tool for targeting tumor cells. The folate receptor, or folate-binding protein (FBP), is overexpressed in a variety of epithelial carcinomas (2). Folate receptor is a glycoprotein receptor anchored to the cell membranes and exhibits a high affinity (dissociation constant,  $\sim 10^{-9}$  nmol/L) for folic acid (3–5). Upon binding to folate receptor, folic acid is transferred into the cells via endocytosis (6,7). Folate receptor is restricted in normal human tissues (8) but has significant levels of expression in thyroid, choroid plexus, and kidneys (9). In contrast, the so-called reduced folate carrier is a low-affinity membrane-spanning protein and is expressed ubiquitously in normal tissues (10).

A number of  $^{111}\text{In}$ -,  $^{66/67/68}\text{Ga}$ -, and  $^{99\text{m}}\text{Tc}$ -folate–based radiopharmaceuticals have been synthesized and successfully evaluated as diagnostic agents for imaging folate receptor–positive tumors. The most widely studied derivatives were labeled either with  $^{111}\text{In}$  or with  $^{99\text{m}}\text{Tc}$  (11,12). A folic acid radiopharmaceutical labeled with  $^{18}\text{F}$  would be of great interest because, compared with other radionuclides,  $^{18}\text{F}$  has excellent imaging characteristics. The half-life of  $^{18}\text{F}$ , 110 min, also allows for syntheses that are more complex and satellite distribution to PET centers with no radiochemistry facilities. The structure of folic acid (compound 1; Fig. 1) does not lend itself to direct radiolabeling with  $^{18}\text{F}$ ; therefore, we sought to functionalize folic acid using 4-fluorobenzylamine as a prosthetic group. Here, we report the synthesis, radiolabeling, and in vitro and in vivo evaluation of the new  $^{18}\text{F}$ -labeled folic acid derivative in nude mice bearing folate receptor–positive tumors.

## MATERIALS AND METHODS

### General

Solvents were purchased from Merck and Fluka and were used without further purification. Chemicals were obtained from Fluka and Bachem. *N*<sup>2</sup>-*N,N*-dimethylaminomethylene-10-formylptericoic acid methyl ester was kindly provided by Merck Eprova AG.

Received Oct. 7, 2005; revision accepted Mar. 21, 2006.

For correspondence or reprints contact: Simon M. Ametamey, PhD, Center for Radiopharmaceutical Science of ETH, PSI, and USZ, ETH Hönggerberg Wolfgang Pauli Strasse 10, CH-8093 Zurich, Switzerland.

E-mail: simon.ametamey@pharma.ethz.ch

COPYRIGHT © 2006 by the Society of Nuclear Medicine, Inc.

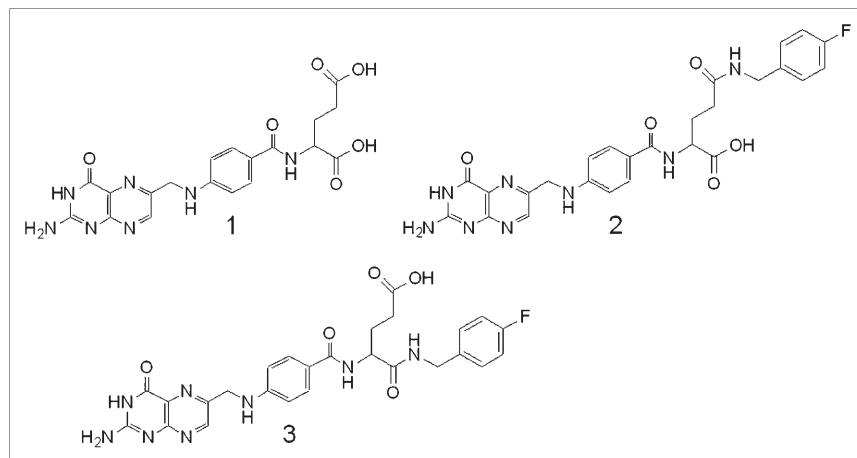


**FIGURE 1.** Native folic acid (compound 1),  $\gamma$ -FBA-folate (compound 2), and  $\alpha$ -FBA-folate (compound 3).

Unlabeled  $\alpha$ - and  $\gamma$ -FBA-folates were synthesized in our laboratory (the synthesis will be reported elsewhere). An Extralut 3 column was obtained from Merck. High-performance liquid chromatography (HPLC) analysis and purification were performed on a Merck-Hitachi L-6200A provided with a  $\gamma$ -counter. The HPLC system used for the semipreparative purification consisted of a Waters 510 pump, a Knauer ultraviolet detector, and a Geiger Müller LND 714 counter with an Eberlein RM-14 instrument.  $^3\text{H}$ -Folic acid potassium salt (37 MBq/mL, 888 GBq/mmol) was purchased from Amersham Biosciences. The scintillation solution, Ultima Gold high-flash-point liquid scintillation cocktail, was purchased from Packard Co. KB-31 cells (CCL-17) were purchased from American Type Culture Collection. Special RPMI cell culture medium (without folic acid, vitamin B<sub>12</sub>, phenol red) was purchased from Cell Culture Technologies GmbH. Radioactivity ( $\beta$ -radiation of  $^3\text{H}$ ) was measured with a  $\beta$ -counter (TRI-CARB, 1900 TR, liquid scintillation analyzer; Packard). Protein concentrations for the in vitro experiments were measured with a microplate reader (model 550; Bio-Rad), using a Micro BCA protein assay kit (Socochem). Experimentally acquired raw data were transformed using Prism software (GraphPad).

### Synthesis of Compound 5

4-(Dimethylamino)benzotrile (2 g, 13.7 mmol) and methyl trifluoromethane triflate (2.15 mL, 19.0 mmol) were refluxed for 6 h under an argon atmosphere. The orange solid residue was isolated by filtration and dissolved in 250 mL of water. The aqueous solution was extracted with  $\text{CH}_2\text{Cl}_2$  ( $2 \times 200$  mL) and thereafter concentrated to dryness. Compound 5 was crystallized from  $\text{CH}_3\text{OH}/\text{AcOEt}$  (87% yield). Analytic data for 5:  $^1\text{H}$  nuclear magnetic resonance (dimethyl sulfoxide [ $\text{DMSO}$ ]- $d_6$ ):  $\delta$ : 3.63 (s, 9 H), 8.19 (s, 4 H). Mass spectrometry (matrix-assisted laser desorption/ionization):  $m/z$ : (161.4)  $[\text{M}]^+$ .

### Radiochemistry

**Production of  $^{18}\text{F}^-$ .**  $^{18}\text{F}^-$  was obtained via the  $^{18}\text{O}(\text{p},\text{n})^{18}\text{F}$  reaction on 98% enriched  $^{18}\text{O}$ -water. Aqueous  $^{18}\text{F}^-$  was transferred into a tightly closed 10-mL Reacti-Vial (Pierce Biotechnology, Inc.) containing 19–20 mg of Kryptofix K<sub>222</sub> (Merck) and 2–3 mg of  $\text{K}_2\text{CO}_3$  dissolved in MeCN (0.5 mL) and 1.5  $\mu\text{L}$  of bidistilled water.

**Synthesis of  $^{18}\text{F}$ - $\alpha/\gamma$ -FBA-Folate (Compounds 7 and 8).** The preparation of the  $^{18}\text{F}$ -Kryptofix-K<sub>222</sub> complex was performed

under standard conditions (13). Briefly, aqueous  $^{18}\text{F}^-$  solution was concentrated to dryness at 115°C under a nitrogen stream for 10–15 min. The residue was dissolved in anhydrous MeCN (1 mL), and the solvent was evaporated to dryness at 115°C under a nitrogen stream. This procedure was repeated twice. Five to 6 mg of compound 5 that had been dissolved in anhydrous DMSO (300  $\mu\text{L}$ ) were added to the Reacti-Vial containing the  $^{18}\text{F}$ -Kryptofix-K<sub>222</sub> and heated to 115°C for 20 min. The reaction mixture was quenched by adding 3 mL of bidistilled water, and the resulting solution was eluted through a *t*-C18 Sep-Pak cartridge (Millipore Corp.). The cartridge was washed with 0.5 mL of water and dried with  $\text{N}_2$  flow over 10 min.  $^{18}\text{F}$ -4-Fluorobenzonitrile was eluted from the cartridge with tetrahydrofuran (THF) (3 mL) and collected in a 10-mL Reacti-Vial containing a 0.6-g molecular sieve (3-Å pore diameter) named RVB. After 5 min at room temperature, the THF solution was transferred to a 10-mL Reacti-Vial named RVC. RVB was washed with THF ( $2 \times 0.5$  mL), and the washing fractions were also transferred to RVC. A saturated THF solution of  $\text{LiAlH}_4$  (0.9 mL) was added dropwise to RVC, which was heated at 120°C for 20 min. After cooling to room temperature, 0.5 mL of bidistilled water was added. After the addition of THF (1 mL), the suspension in RVC was transferred to an Extralut 3 cartridge. RVC was washed twice with THF (1 mL), and the washings were loaded to the same cartridge.  $^{18}\text{F}$ -4-Fluorobenzylamine (compound 6) was eluted from the cartridge with  $\text{CH}_2\text{Cl}_2$  (6 mL) and collected in a 10-mL Reacti-Vial named RVD. The solvent was evaporated at room temperature under a weak  $\text{N}_2$  flow. In a separate vial, a suspension of folic acid (3 mg, 6.8  $\mu\text{mol}$ ) and 1-hydroxybenzotriazole (HOBt) (0.9 mg, 6  $\mu\text{mol}$ ) in DMSO (300  $\mu\text{L}$ ) and *N*-(3-dimethylaminopropyl)-*N*-ethylcarbodiimide (1.5 mg, 7.8  $\mu\text{mol}$ ) in DMSO (300  $\mu\text{L}$ ) was added 5 min before the final coupling reaction. The DMSO solution containing the activated folic acid was added to RVD, and the coupling reaction was performed by heating at 100°C for 30 min. The reaction mixture was quenched with 1 mL of HPLC eluent (23%  $\text{CH}_3\text{OH}$ , 77%  $\text{NH}_4\text{HCO}_3$  [pH 7]).  $^{18}\text{F}$ -labeled compound was purified using the following semipreparative HPLC conditions: Spherisorb 5 ODS 1 (Phenomenex) column, 250  $\times$  10 mm; isocratic elution (flow, 3 mL/min); eluent, 23%  $\text{CH}_3\text{OH}$ , 77%  $\text{NH}_4\text{HCO}_3$  (pH 7). The fraction containing the product was collected. After evaporation, the product was formulated using a 0.15 mol/L concentration of phosphate buffer and filtered through a 0.22- $\mu\text{m}$  Millipore filter.

## Analytic HPLC

Quality control was performed using a SphereClone 5 $\mu$  ODS(1) (250  $\times$  4.60 mm; Phenomenex) column and applying a linear gradient of HPLC eluents A and B. Eluent A consisted of 90% NH<sub>4</sub>HCO<sub>3</sub> (0.05 mol/L [pH 7]) and 10% CH<sub>3</sub>OH; eluent B consisted of 100% CH<sub>3</sub>OH. A typical HPLC analytic gradient was 20%–50% B over 30 min, at a flow of 0.8–1 mL/min. The  $\gamma$ - and  $\alpha$ -isomers of the <sup>18</sup>F-labeled folate conjugate were separated using the following analytic HPLC conditions: SphereClone 5 $\mu$  ODS(1) (250  $\times$  4.60 mm; Phenomenex) column; eluent A, 95% trimethylammonium phosphate [pH 3.5] and 5% CH<sub>3</sub>OH; eluent B, 100% CH<sub>3</sub>OH; linear gradient, 0%–50% B or 0%–80% B over 30 min; flow, 0.8–1 mL/min.

## Cell Cultures

KB-31 cells (human nasopharyngeal epidermal carcinoma cell line overexpressing the folate receptor) were cultured continuously as monolayers in 75-cm<sup>2</sup> flasks at 37°C in a humidified atmosphere containing 7.5% CO<sub>2</sub>. The cells were folate starved using a folate-deficient RPMI 1640 medium (modified RPMI 1640 without folic acid, vitamin B12, and phenol red) supplemented with 10% heat-inactivated fetal calf serum (as the only source of folate) containing L-glutamine and antibiotics (penicillin, 100 IU/mL; streptomycin, 100  $\mu$ g/mL; amphotericin B, 0.25  $\mu$ g/mL). Cell culture media such as fetal calf serum-supplemented folate-deficient RPMI 1640 are known to feature a final folate concentration of approximately 3 nmol/L, that is, a value at the low end of the physiologic concentration in human serum (14).

*Preparation of Cells for In Vitro Experiments.* Eighteen to 20 h before each experiment, the cells were seeded into 12-well plates (6.5  $\times$  10<sup>5</sup> cells per well) to form subconfluent monolayers overnight. Experiments were performed in triplicate for each concentration.

*Preparation of Cells for In Vivo Experiments.* For subcutaneous inoculation into the mice, subconfluent cells were harvested by treatment with ethylenediaminetetraacetic acid (1 mmol/L) in phosphate-buffered saline (PBS; 1 $\times$  [pH 7.4]). The cells were then washed once with PBS and pelleted by being spun at 1,000g for 5 min at 20°C. The cells were resuspended in PBS for inoculation.

## Determination of Inhibitory Concentration of 50% (IC<sub>50</sub>)

Cell-binding experiments using <sup>3</sup>H-folic acid were performed according to the following general procedure: The monolayers were rinsed twice with ice-cold PBS (pH 7.4). Pure, ice-cold folate-deficient RPMI 1640 medium (without fetal calf serum, L-glutamine, and antibiotics) (475  $\mu$ L) was added to each well. Five hundred microliters of the corresponding ice-cold solution of native folic acid (20 concentrations or, for compounds 2 and 3, 14 concentrations) were added. The well plates were preincubated at 4°C for 40 min. This incubation temperature was chosen to minimize endocytosis of folate receptor. A solution of <sup>3</sup>H-folic acid (25  $\mu$ L,  $\sim$ 0.74 kBq/ $\mu$ L) was added and the well plates incubated again on ice at 4°C for 2 h. Preliminary experiments showed that 2 h is an optimal incubation time and that saturation of cell binding is almost reached at that time point. Each well was rinsed 3 times with ice-cold PBS (pH 7.4). The monolayers were dissolved in 1N NaOH (1,000  $\mu$ L), transferred in 4-mL tubes, and homogenized by a vortex mixer. Scintillation solution (4 mL) was added to each sample, homogenized, and transferred into scintillation flacons to be counted for radioactivity using a  $\beta$ -counter.

The IC<sub>50</sub> values were calculated directly from the corresponding data using the Prism software. For native folic acid, the mean IC<sub>50</sub> was determined in 2 independent experiments, whereas for compounds 2 and 3, 3 independent experiments were performed. The Student *t* test (unpaired, unequal variance) was used to determine whether there was a significant difference between IC<sub>50</sub> values.

## In Vivo Studies

*Animals.* Animal studies complied with Swiss laws on animal protection, and housing and animal husbandry complied with local laws on animal protection. Five- to 6-wk-old female nude mice (CD1-Foxn1<sup>tmu</sup>) were purchased from Charles River. The mice were housed at a controlled temperature (26°C), humidity (68%), and daily light cycle (12 h light/12 h dark) and were maintained on a folate-deficient rodent diet (to reduce their serum folate to a level near that of human serum) (15). After a 7- to 14-d acclimatization period, 0.1 mL of KB-31 tumor cell suspension (50  $\times$  10<sup>6</sup> cells/mL) was inoculated into the subcutis of the right and left axilla of each mouse. The animal experiments were performed 10–12 d after the tumor cell inoculation, when the tumors had reached weights of 200–500 mg.

*Biodistribution Study by Dissection.* The mice received an injection of <sup>18</sup>F- $\alpha$ / $\gamma$ -FBA-folate (0.33–0.81 MBq; maximum volume, 150  $\mu$ L) via a lateral tail vein. Ten minutes before tracer administration, the blockage group (*n* = 4) received an intravenous injection of 200  $\mu$ g of folic acid (dissolved in 100  $\mu$ L of phosphate buffer), whereas the control group (*n* = 4) received an intravenous injection of 100  $\mu$ L of phosphate buffer. At 125 min after injection, the animals were sacrificed by decapitation and dissected. Tumors and organs were removed, rinsed with phosphate buffer, dried with a piece of tissue paper, and measured together with an aliquot of the injected solution in a  $\gamma$ -counter (Wizard; PerkinElmer) using an energy window of 300–700 keV. Results were expressed as percentage injected dose per gram of tissue (%ID/g; ((cpm organ/g organ)/cpm injected)  $\times$  100).

*PET Imaging.* PET experiments were performed with the 16-module variant of the quad-HIDAC tomograph (Oxford Positron Systems), the performance of which has been reported elsewhere (16,17). A most important characteristic of this dedicated small-animal PET system is an ultrahigh resolution of less than 0.9 mm<sup>3</sup>. The animals, which were awake, were lightly restrained and intravenously injected with the radioligand via a lateral tail vein. At various times after injection, the animals were anesthetized with isoflurane (Abbott) in an air/oxygen mixture and positioned in the PET camera as described previously (18).

Initial PET studies with the <sup>18</sup>F-labeled folic acid derivative were performed to determine the PET protocol that would most clearly show tumors in nude mice (*n* = 4) bearing KB-31 tumor xenografts. Visual inspection of PET images obtained at various times after injection (30, 75, 120, and 165 min) revealed that tumor accumulation was highest when data acquisition began at 75 min after injection.

For a comparison of <sup>18</sup>F-FDG uptake with <sup>18</sup>F- $\alpha$ / $\gamma$ -FBA-folate uptake, a single animal was initially injected with 16.9 MBq of <sup>18</sup>F-FDG and scanned from 30 to 60 min after injection. Two days later, the same animal was imaged again 75 min after injection of 13.3 MBq of the <sup>18</sup>F-folate derivative (scan duration, 45 min).

For a demonstration of the in vivo binding specificity of the radioligand, a single mouse was scanned first under control conditions (100  $\mu$ L of phosphate buffer injected 10 min before

16.9 MBq of the radioligand) and again 24 h later under blockage conditions (200  $\mu$ g of folic acid injected 10 min before 13.9 MBq of radioligand). Both PET scans were initiated 75 min after injection of the tracer and lasted for 45 min.

PET data were acquired in list mode and reconstructed in a single time frame using the fast, accurate iterative reconstruction algorithm with a 0.5-mm bin and a  $200 \times 200 \times 240$  matrix (19). Reconstruction did not include correction for scatter, randoms, or attenuation. Image files were normalized to the injected dose per body weight and analyzed using the dedicated software PMod (20).

## RESULTS

### Radiochemistry

$^{18}\text{F}$  labeling was performed by no-carrier-added nucleophilic radiofluorination on 4-cyano-*N,N*,*N*-trimethylanilinium trifluoromethane sulfonate (Fig. 2) using the same conditions as those reported by Dolle et al. (21). 4- $^{18}\text{F}$ -Benzonitrile was purified over a C18 Sep-Pak cartridge, and the nitrile functionality was reduced to that of the corresponding amine using a saturated THF solution of  $\text{LiAlH}_4$  instead of dry, powdered  $\text{LiAlH}_4$ . The  $^{18}\text{F}$ -labeled prosthetic group was isolated by extraction with an Extralut 3 cartridge with a radiochemical yield (decay corrected) ranging from 8% to 13%. The final step of the synthesis, an in situ generation of activated folic acid, was accomplished using *N*-(3-dimethylaminopropyl)-*N*-ethyl-carbodiimide and HOBt 5 min before initiation of the coupling reaction. The yield of the coupling step after HPLC purification ranged from 15% to 44% (decay corrected), and the specific radioactivity ranged from 7 to 24 GBq/ $\mu\text{mol}$ . The product (a mixture of  $\alpha$ - and  $\gamma$ -isomers) eluted as a broad peak with a retention time of 25 min.

$^{18}\text{F}$ -labeled FBA-folate was characterized by analytic HPLC by coinjection with a reference compound ( $\gamma$ -FBA-folate) using an eluent buffered to pH 7. Under these conditions, only 1 radioactive peak was observed (data not

shown). In contrast, at pH 3.5, 2 distinct radioactive peaks corresponding to the  $\gamma$ - and  $\alpha$ -isomers were identified (Fig. 3). The  $\gamma/\alpha$ -isomeric ratio was 4:1.

### Binding Assays

As reported in a previous investigation (12), the cells were grown in folate-deficient medium to reproduce a folic acid concentration similar to that of human plasma. The  $\text{IC}_{50}$  values were obtained by inhibition experiments using  $^3\text{H}$ -folic acid. Three representative binding curves are shown in Figure 4. The mean  $\text{IC}_{50}$  values for the  $\alpha$ - and  $\gamma$ -regioisomers were  $71 \pm 8$  and  $62 \pm 6$  nmol/L, respectively, suggesting that the binding affinities of the  $\alpha$ - and  $\gamma$ -regioisomers do not significantly differ ( $P > 0.05$ ) and are comparable to that of native folic acid ( $\text{IC}_{50} = 41$  nmol/L;  $P > 0.05$ ).

### In Vivo Studies

The high resolution of the quad-HIDAC camera allowed visualization of heterogeneous tracer uptake within the tumor (Fig. 5). Higher activity concentrations were observed in the tumor rim, suggesting increased perfusion or folate receptor expression in this region. For a direct comparison of  $^{18}\text{F}$ -FDG with  $^{18}\text{F}$ - $\alpha/\gamma$ -FBA-folate, a tumor-bearing mouse was scanned after injection of  $^{18}\text{F}$ -FDG and rescanned 2 d later after injection of the  $^{18}\text{F}$ -labeled folic acid derivative. The PET images in Figure 5 represent corresponding coronal whole-body sections through the tumor and clearly demonstrate the utility of the  $^{18}\text{F}$ -labeled folic acid derivative for visualizing KB-31 tumor xenografts.  $^{18}\text{F}$ -FDG accumulation in this KB-31 tumor model was only marginal (18).

The whole-body distribution of  $^{18}\text{F}$ - $\alpha/\gamma$ -FBA-folate was then assessed by PET from 75 to 120 min after injection. Figure 6 shows a series of coronal slices from ventral to dorsal through the whole body of the mouse. Both the

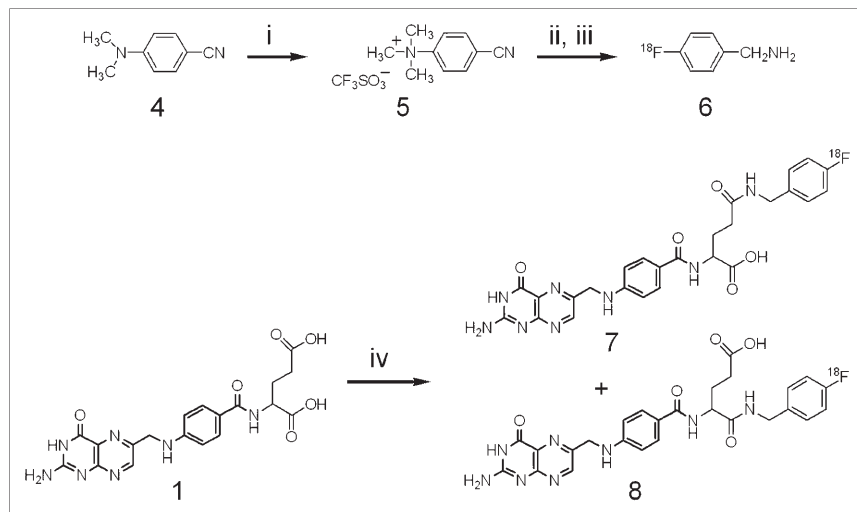


**FIGURE 2.** Radiosynthesis of  $^{18}\text{F}$ -labeled  $\alpha$ - and  $\gamma$ -FBA-folate: (i) methyl trifluoromethane triflate, argon atmosphere, reflux, 6 h; (ii)  $^{18}\text{F}$ -Kryptofix- $\text{K}_{222}$ , DMSO  $120^\circ\text{C}$ , 20 min; (iii)  $\text{LiAlH}_4$ , THF,  $120^\circ\text{C}$ , 12 min; (iv) 1, *N*-(3-dimethylaminopropyl)-*N*-ethyl-carbodiimide, HOBt, DMSO,  $100^\circ\text{C}$ , 30 min.

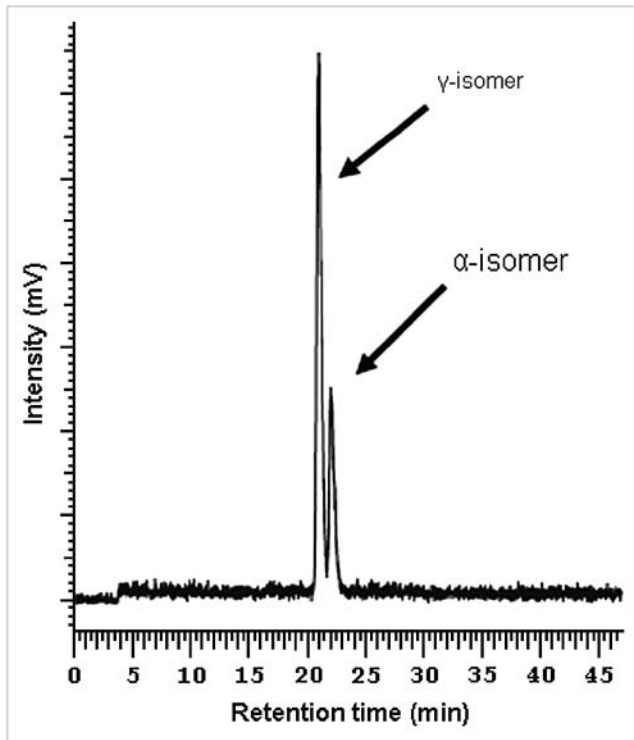


**FIGURE 3.** Analytic HPLC of  $^{18}\text{F}$ -labeled folic acid derivative as obtained after semipreparative HPLC purification and formulation. Column: SphereClone  $5\mu$ . ODS(1) ( $250 \times 4.6$  mm; Phenomenex); eluent A: 95% trimethylammonium phosphate (pH 3.5) and 5%  $\text{CH}_3\text{OH}$ ; eluent B: 100%  $\text{CH}_3\text{OH}$ ; linear 0%–80% B over 30 min; flow: 0.8 mL/min.

hepatobiliary and the renal elimination pathways of the radioligand dominated the whole-body distribution pattern, with the highest activity concentrations in the gallbladder, urinary bladder, and parts of the intestines. Moderate activity accumulation was evident in the kidneys, tumors, and liver.

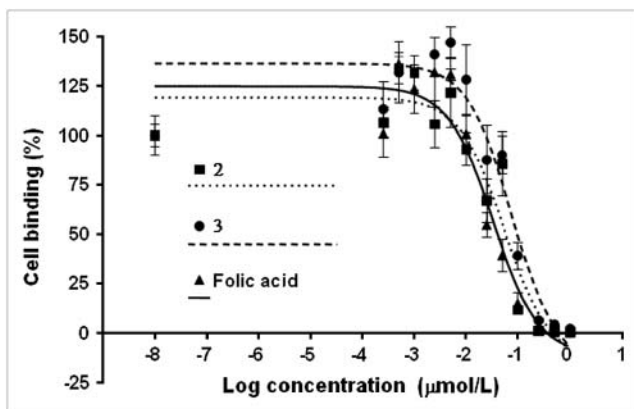


**FIGURE 4.** Determination of  $\text{IC}_{50}$  values using KB-31 cells (human nasopharyngeal epidermal carcinoma cell line over-expressing folate receptor): inhibition of  $^3\text{H}$ -folic acid with folic acid and folic acid derivatives 2 and 3. Curves do not correspond to values in Table 1 representing average of different experiments.

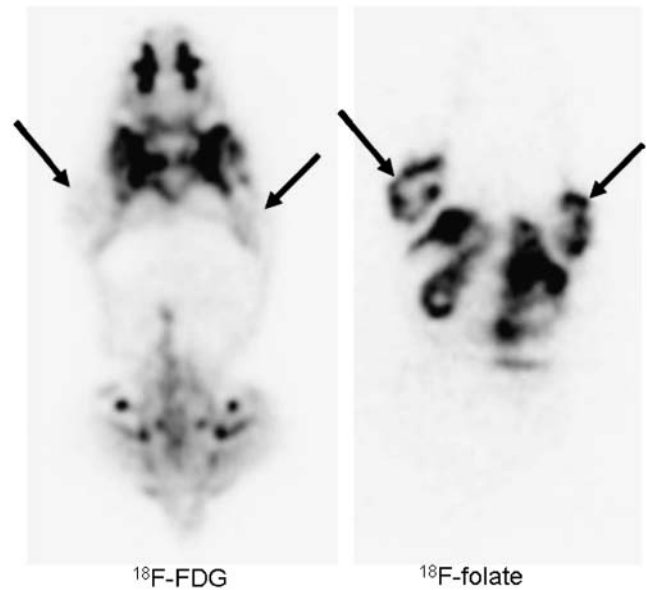


**FIGURE 5.** PET imaging of  $^{18}\text{F}$ -FDG vs.  $^{18}\text{F}$ - $\alpha/\gamma$ -FBA-folate in same animal: Athymic nude mouse (24.5 g) on folate-free diet with 2 KB-31 tumors located dorsally on right and left sides of upper thorax (arrows) was scanned 30 min after injection of 16.9 MBq of  $^{18}\text{F}$ -FDG (scan duration, 30 min). Two days later, same animal was imaged again 75 min after injection of 13.3 MBq of  $^{18}\text{F}$ -labeled folate derivative (scan duration, 45 min). PET images represent corresponding coronal whole-body sections through tumor. Moderate  $^{18}\text{F}$ -FDG uptake was observed in various muscles, whereas for  $^{18}\text{F}$ -labeled folate derivative, highest accumulation of radioactivity was observed in liver and kidneys.

To demonstrate the specificity of radioligand binding to the folate receptor-positive KB-31 tumor xenografts, we performed classic postmortem biodistribution studies under baseline and blockage conditions. The blockage group received 200  $\mu\text{g}$  of folic acid 10 min before the radioligand, and the control group was injected with a corresponding volume of phosphate buffer. Radioactivity uptake in tumors at 125 min after injection amounted to 6.56 %ID/g in control animals, whereas radioactivity accumulation in the tumors of blockage animals was significantly reduced by more than 80%—to 1.07 %ID/g (Table 1;  $P = 0.001$ ). An even larger blockage effect (>97%) was observed in the kidneys, where radioactivity uptake was reduced from 40.65 to 1.16 %ID/g. The highest accumulation of activity in control animals was found in bile, urine, and feces, thus confirming the distribution pattern revealed by PET (Fig. 6).

The in vivo binding specificity of  $^{18}\text{F}$ - $\alpha/\gamma$ -FBA-folate to the folate receptor on KB-31 tumor cells was also demonstrated by PET. A nude mouse with 2 KB-31 tumors was scanned under control conditions and imaged 24 h later under blockage conditions. Both PET scans were initiated 75 min after injection of the radiotracer and lasted for 45 min. Figure 7 shows PET images of corresponding coronal whole-body sections through the KB-31 tumors and

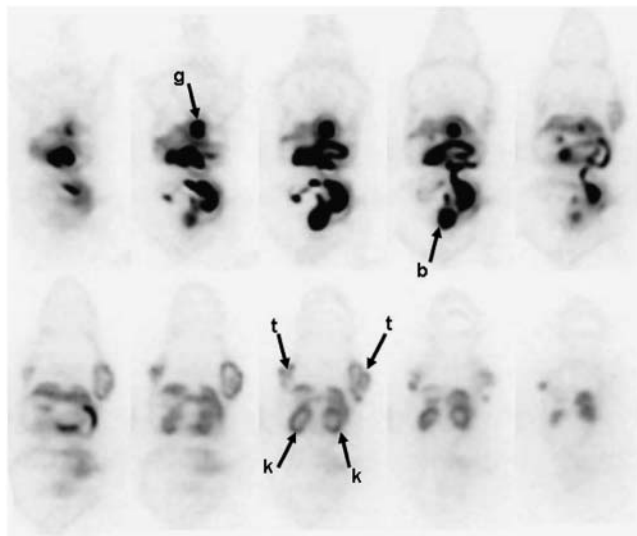


**FIGURE 6.** Whole-body distribution of  $^{18}\text{F}$ - $\alpha/\gamma$ -FBA-folate visualized on PET: Athymic nude mouse (22.9 g) on folate-free diet was injected with 12.5 MBq of radiotracer and scanned for 45 min at 75 min after injection. PET images represent series of coronal slices of a single experiment from ventral through whole body of mouse. b = bladder; g = gallbladder; k = kidneys; t = KB-31 tumors.

through the kidneys under both experimental conditions. Tumors and kidneys were visualized only in the absence of competing folic acid, supporting the specificity of  $^{18}\text{F}$ - $\alpha/\gamma$ -FBA-folate binding to the folate receptor in vivo.

## DISCUSSION

Tumor imaging with  $^{18}\text{F}$ -FDG, the most widely used PET tracer, is hampered by false-positive findings. A

**TABLE 1**

Postmortem Biodistribution Study of  $^{18}\text{F}$ - $\alpha/\gamma$ -FBA-Folate at 125 Minutes After Injection in Athymic Nude Mice

Tissue	Control	Blockade*
Tumor	6.56 ± 1.80	1.07 ± 0.38
Blood	1.43 ± 0.46	1.29 ± 0.51
Kidney	40.65 ± 12.81	1.16 ± 0.41
Liver	2.37 ± 0.42	3.05 ± 2.24
Lung	1.16 ± 0.73	0.82 ± 0.20
Brain	0.26 ± 0.10	0.15 ± 0.07
Spleen	0.34 ± 0.05	0.54 ± 0.37
Stomach	0.34 ± 0.03	0.22 ± 0.01
Heart	0.80 ± 0.12	0.60 ± 0.16
Duodenum	5.01 ± 2.01	4.88 ± 1.56
Bone	0.51 ± 0.14	0.90 ± 0.74
Muscle	0.37 ± 0.07	0.76 ± 0.82
Urine	130.71 ± 92.52	84.92 ± 41.63
Bile	265.80 ± 164.13	326.29 ± 14.66
Feces	29.54 ± 19.98	29.44 ± 25.80

\*200  $\mu\text{g}$  of cold folate.  
Data are %ID/g.

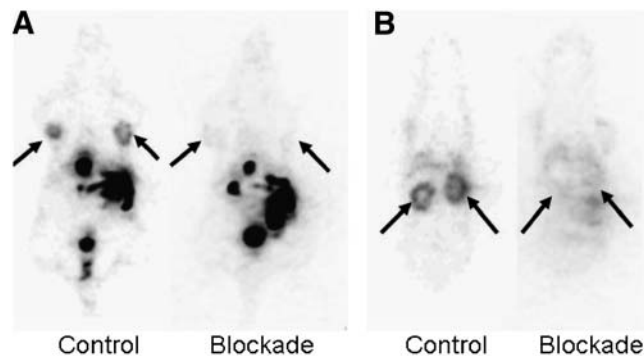


**FIGURE 7.** In vivo binding specificity of  $^{18}\text{F}$ - $\alpha/\gamma$ -FBA-folate: Athymic nude mouse (24.5 g) on folate-free diet with 2 KB-31 tumors was scanned after radiotracer injection under control conditions (100  $\mu\text{L}$  of phosphate buffer injected 10 min before radiotracer) and 24 h later under blockage conditions (200  $\mu\text{g}$  of folic acid injected 10 min before radiotracer). Both PET scans were initiated 75 min after injection of tracer and lasted for 45 min. PET images represent corresponding coronal whole-body sections through KB-31 tumors (A; arrows) and through kidneys (B; arrows) and are normalized to injected dose per body weight.

receptor-mediated uptake is an attractive approach for tumor imaging because this approach involves cell-selective radiopharmaceutical targeting. The folate receptor is known to be overexpressed in a variety of human epithelial carcinomas (2), making these tumors excellent targets for diagnostic imaging with radiolabeled folic acid conjugates. But for folate conjugates, it is still unclear whether a free  $\alpha$ -carboxyl group is necessary for retaining binding to the folate receptor (12,22), and thus we found it necessary to prepare well-defined unlabeled  $\gamma$ - and  $\alpha$ -folic acid derivatives to clarify this point. The binding experiments performed on the unlabeled  $\gamma$ - and  $\alpha$ -FBA-folates using  $^3\text{H}$ -folic acid indicated that both regioisomers exhibited similar binding affinities to KB-31 cells, corroborating previous data obtained with  $^{99\text{m}}\text{Tc}$ -folate derivatives (12) and suggesting further that linking a prosthetic group such as 4-fluorobenzylamine to folic acid via either the  $\gamma$ - or the  $\alpha$ -carboxylate does not have a detrimental effect on the binding affinity of the corresponding folate conjugate. These data encouraged us to pursue the  $^{18}\text{F}$  labeling of folic acid. It is important to note that the synthetic procedure (Fig. 2) adopted for the  $^{18}\text{F}$ -labeled folic acid derivative is different from the method used in the synthesis of the unlabeled  $\gamma$ - and  $\alpha$ -FBA-folates. The radiochemical yield obtained for  $^{18}\text{F}$ -4-fluorobenzylamine was in the range of 8%–13%. The coupling step was accomplished using standard coupling reagents and gave, after HPLC purification, satisfactory radiochemical yields. However, the overall radiochemical yield was low because of material loss during purification of the prosthetic group. The use of a cartridge containing the same type of material but of reduced size may improve the yield of this step and, consequently, the overall radiochemical yield. The difference in the pKa value of the  $\gamma$ - and  $\alpha$ -carboxyl-groups (23)

allowed us to distinguish between the 2 regioisomers using analytic HPLC at pH 3.5 (Fig. 3), with the major peak being the  $\gamma$ -regioisomer. More detailed investigations are, however, required to determine whether the predominance of the  $\gamma$ -derivative is due to a rearrangement that progressively converts the  $\alpha$ -isomer to the more thermodynamically stable  $\gamma$ -isomer. The analytic HPLC method used to distinguish the 2 regioisomers may potentially be used for the semipreparative purification; however, this use is not practicable because of the insolubility of the folic acid derivative at pH 3.5.

The  $^{18}\text{F}$ -FDG studies on a nude mouse were performed to compare  $^{18}\text{F}$ -FDG uptake with the new  $^{18}\text{F}$ -labeled folic acid derivative but found no significant accumulation of  $^{18}\text{F}$ -FDG in the KB-31 tumor-bearing mouse. With our new  $^{18}\text{F}$ -labeled folic acid derivative, KB-31 tumors were clearly visualized. The high-resolution quad-HIDAC tomograph permitted the delineation of heterogeneous tracer uptake within the tumor. The highest accumulation of activity was in the tumor rim, but even this peripheral zone of the tumor revealed a spotted distribution pattern (Fig. 5), suggesting heterogeneous folate receptor expression or perfusion in this region. Because of a prominent hepatobiliary elimination of the radiotracer, high activity concentrations were observed in the gallbladder and, consequently, in the intestines. These high concentrations may be problematic for clear visualization of abdominal tumors near the intestines, bladder, or kidneys. Hepatobiliary and renal elimination of the radioligand was also evident from post-mortem dissection studies. As expected from the distribution pattern observed on PET, the highest activity concentrations were observed in bile, urine, feces, and kidneys (Table 1). Apart from these locations, the KB-31 tumors showed the highest radioactivity uptake (6.56 %ID/g at 125 min after injection). Tumor-to-blood and tumor-to-liver ratios amounted to 4.6 and 2.8, respectively. Other tumor-to-organ ratios gave even higher values. The in vivo specificity of the new ligand was confirmed by a repeated PET study on a single animal within 24 h, first under baseline conditions and then under blockage conditions. The comparison of normalized PET images proved the specificity of tracer binding in the tumors and the kidneys (Fig. 7). The specificity of binding to folate receptor was also clearly demonstrated by classic postmortem biodistribution studies. The dissection experiments revealed a highly significant difference in %ID/g values for tumors and kidneys, resulting in a blockage of 84% and 97%, respectively. The larger value for kidneys may be explained by a higher target protein density in kidneys or a higher nonspecific tracer accumulation in tumors. The high degree of specific binding observed in the folate receptor-positive tumors and the kidneys confirms previous data obtained with  $^{99\text{m}}\text{Tc}$ -folate derivatives (9) and shows that this new PET ligand is also capable of efficiently imaging folate receptor-positive tumors in an animal model. Because folate receptors are significantly overexpressed in most

human tumors, this new  $^{18}\text{F}$ -labeled folate derivative may be a promising diagnostic tool for investigating folate receptor-positive tumors in humans using PET. For some selected human tumors in which the use of  $^{18}\text{F}$ -FDG is unsatisfactory, folate receptor-targeted radiopharmaceuticals may show promise.

## CONCLUSION

$\gamma$ -FBA-folate and  $\alpha$ -FBA-folate were evaluated in vitro. Both regioisomers exhibited similar binding affinities, which were comparable to that of parent folic acid. We also established a method for the  $^{18}\text{F}$  labeling of folic acid. The method uses commercially available folic acid as a precursor and circumvents time-consuming chemical modifications of the native compound such as protection/deprotection. In vivo studies indicated that the new radioligand binds selectively to folate receptor-positive KB-31 tumor xenografts. Therefore, this new  $^{18}\text{F}$ -labeled folic derivative is a promising tool for PET imaging of folate receptor-positive tumors.

## ACKNOWLEDGMENTS

We thank Andy Isenschmid and Yvonne Eichholzer for the  $^{18}\text{F}^-$  production; Cecile Dumas, Alain Blanc, and Marie-Line Lehaire for the nuclear magnetic resonance and mass spectrometry measurements; Claudia Keller and Matthias Wyss for support with the in vivo studies; and Anass Johayem for technical support.

## REFERENCES

1. Leamon C, Low PS. Folate-mediated targeting: from diagnostic to drug and gene delivery. *Drug Discov Today*. 2001;6:44–51.
2. Garin-Chesa P, Campbell I, Saigo PE, Lewis JL Jr, Old LJ, Rettig WJ. Sensitivity and specificity in immunopathology and molecular identification as a folate-binding protein. *Am J Pathol*. 1993;142:557–567.
3. McHugh M, Cheng YC. Demonstration of a high affinity folate binder in human cell membranes and its characterization in cultured human KB cells. *J Biol Chem*. 1979;254:11312–11318.
4. Kamen B, Capdevila A. Receptor mediated folate accumulation is regulated by the cellular folate content. *Proc Natl Acad Sci U S A*. 1986;83:5983–5987.
5. Kane MA, Waxman S. Role of the folate binding proteins in folate metabolism. *Lab Invest*. 1989;60:737–746.
6. Westerhof G, Schornagel JH, Kathmann I, et al. Carrier- and receptor-mediated transport of folate antagonists targeting folate-dependent enzymes: correlates of molecular-structure and biological activity. *Mol Pharmacol*. 1995;48:459–471.
7. Rothberg K, Ying YS, Kolhouse JF, Kamen BA, Anderson RG. The glycopospholipid-linked folate receptor internalizes folate without entering the clathrin-coated pit endocytic pathway. *J Cell Biol*. 1990;110:637–649.
8. Weitman S, Lark RH, Coney LR, et al. Distribution of the folate receptor GP38 in normal and malignant cell lines and tissues. *Cancer Res*. 1992;52:3396–3401.
9. Ke C, Mathias CJ, Green MA. The folate receptor as a molecular target for tumor-selective radionuclide delivery. *Nucl Med Biol*. 2003;30:811–817.
10. Antony A. The biological chemistry of folate receptors. *Blood*. 1992;79:2807–2820.
11. Siegel B, Dehdashti F, Mutch DG, et al. Evaluation of  $^{111}\text{In}$ -DTPA-folate as a receptor targeted diagnostic agent for ovarian cancer: initial clinical results. *J Nucl Med*. 2003;44:700–707.
12. Müller C, Dumas C, Hoffmann U, Schubiger PA, Schibli R. Organometallic  $^{99\text{m}}\text{Tc}$ -technetium(I)- and Re-rhenium(I)-folate derivatives for potential use in nuclear medicine. *J Organomet Chem*. 2004;689:4712–4721.
13. Sannick S, Ametamey SM, Leenders KL, et al. Electrophysiological study, biodistribution in mice and preliminary PET evaluation in a rhesus monkey of

- 1-amino-3-[<sup>18</sup>F]fluoromethyl-5-methyl-adamantane (<sup>18</sup>F-MEM): a potential radioligand for mapping the NMDA-receptor complex. *Nucl Med Biol.* 1998; 25:323–330.
14. Antony AC, Kane MA, Portillo RM, Elwood PC, Kolhouse JF. Studies of the role of a particulate folate-binding protein in the uptake of 5-methyltetrahydrofolate by cultured human KB cells. *J Biol Chem.* 1985;260:4911–4917.
  15. Mathias CJ, Wang S, Lee RJ, Waters DJ, Low PS, Green MA. Tumor-selective radiopharmaceutical targeting via receptor-mediated endocytosis of gallium-67-deferoxamine-folate. *J Nucl Med.* 1996;37:1003–1008.
  16. Jeavons AP, Chandler RA, Dettmar CAR. A 3D HIDAC-PET camera with sub-millimetre resolution for imaging small animals. *IEEE Trans Nucl Sci.* 1999;46:468–473.
  17. Missimer J, Madi Z, Honer M, Keller C, Schubiger A, Ametamey SM. Performance evaluation of the 16-module quad-HIDAC small animal PET camera. *Phys Med Biol.* 2004;49:2069–2081.
  18. Honer M, Bruhlmeier M, Missimer J, Schubiger AP, Ametamey SM. Dynamic imaging of striatal D-2 receptors in mice using quad-HIDAC PET. *J Nucl Med.* 2004;45:464–470.
  19. Reader AJ, Erlandsson K, Flower MA, Ott RJ. Fast accurate iterative reconstruction for low-statistics positron volume imaging. *Phys Med Biol.* 1998;43:835–846.
  20. Mikolajczyk K, Szabatin M, Rudnicki P, Grodzki M, Burger CA. JAVA environment for medical image data analysis: initial application for brain PET quantitation. *Med Inform (Lond).* 1998;23:207–214.
  21. Dolle F, Hinnen F, Vauffrey F, Tavitian B, Crouzel C. A general method for labeling oligodeoxynucleotides with <sup>18</sup>F for in vivo PET imaging. *J Labelled Compds Radiopharm.* 1997;39:319–330.
  22. Guo W, Hinkle GH, Lee RJ. <sup>99m</sup>Tc-HYNIC-folate: a novel receptor-based targeted radiopharmaceutical for tumor imaging. *J Nucl Med.* 1999;40:1563–1569.
  23. Wang S, Luo J, Lantrip DA, et al. Design and synthesis of [<sup>111</sup>In]DTPA-folate for use as a tumor-targeted radiopharmaceutical. *Bioconjug Chem.* 1997;8:673–679.